# Measurement of the hadronic photon structure function at LEP 1 for $\langle Q^2 \rangle$ values between 9.9 and 284 GeV$^2$

R. Barate, D. Decamp, P. Ghez, C. Goy, J P. Lees, E. Merle, M N. Minard, B. Pietrzyk, R. Alemany, M P. Casado, et al.

EUROPEAN ORGANISATION FOR PARTICLE PHYSICS

CERN-EP/99-063
28 April 1999

# Measurement of the Hadronic Photon Structure Function at LEP 1 for $\langle Q^2 \rangle$ values between 9.9 and 284 GeV$^2$

The ALEPH Collaboration

**Abstract**

Inclusive $\gamma^*\gamma$ interactions to hadronic final states where one scattered electron or positron is detected in the electromagnetic calorimeters have been studied in the LEP 1 data taken by ALEPH from 1991 to 1995. The event sample has been used to measure the hadronic structure function of the photon $F_2^\gamma$ in three bins with $\langle Q^2 \rangle$ of 9.9, 20.7 and 284 GeV$^2$.

(Submitted to Physics Letters)

# The ALEPH Collaboration

R. Barate, D. Decamp, P. Ghez, C. Goy, J.-P. Lees, E. Merle, M.-N. Minard, B. Pietrzyk

*Laboratoire de Physique des Particules (LAPP), IN$^2$P$^3$-CNRS, F-74019 Annecy-le-Vieux Cedex, France*

R. Alemany, M.P. Casado, M. Chmeissani, J.M. Crespo, E. Fernandez, M. Fernandez-Bosman, Ll. Garrido,[15] E. Graugès, A. Juste, M. Martinez, G. Merino, R. Miquel, Ll.M. Mir, A. Pacheco, I.C. Park, I. Riu

*Institut de Física d'Altes Energies, Universitat Autònoma de Barcelona, E-08193 Bellaterra (Barcelona), Spain*[7]

A. Colaleo, D. Creanza, M. de Palma, G. Gelao, G. Iaselli, G. Maggi, M. Maggi, S. Nuzzo, A. Ranieri, G. Raso, F. Ruggieri, G. Selvaggi, L. Silvestris, P. Tempesta, A. Tricomi,[3] G. Zito

*Dipartimento di Fisica, INFN Sezione di Bari, I-70126 Bari, Italy*

X. Huang, J. Lin, Q. Ouyang, T. Wang, Y. Xie, R. Xu, S. Xue, J. Zhang, L. Zhang, W. Zhao

*Institute of High-Energy Physics, Academia Sinica, Beijing, The People's Republic of China*[8]

D. Abbaneo, U. Becker,[19] G. Boix,[6] M. Cattaneo, F. Cerutti, V. Ciulli, G. Dissertori, H. Drevermann, R.W. Forty, M. Frank, A.W. Halley, J.B. Hansen, J. Harvey, P. Janot, B. Jost, I. Lehraus, O. Leroy, P. Mato, A. Minten, A. Moutoussi, F. Ranjard, L. Rolandi, D. Rousseau, D. Schlatter, M. Schmitt,[20] O. Schneider,[23] P. Spagnolo, W. Tejessy, F. Teubert, I.R. Tomalin, E. Tournefier, A.E. Wright

*European Laboratory for Particle Physics (CERN), CH-1211 Geneva 23, Switzerland*

Z. Ajaltouni, F. Badaud, G. Chazelle, O. Deschamps, A. Falvard, C. Ferdi, P. Gay, C. Guicheney, P. Henrard, J. Jousset, B. Michel, S. Monteil, J-C. Montret, D. Pallin, P. Perret, F. Podlyski

*Laboratoire de Physique Corpusculaire, Université Blaise Pascal, IN$^2$P$^3$-CNRS, Clermont-Ferrand, F-63177 Aubière, France*

J.D. Hansen, J.R. Hansen, P.H. Hansen, B.S. Nilsson, B. Rensch, A. Wäänänen

*Niels Bohr Institute, DK-2100 Copenhagen, Denmark*[9]

G. Daskalakis, A. Kyriakis, C. Markou, E. Simopoulou, I. Siotis, A. Vayaki

*Nuclear Research Center Demokritos (NRCD), GR-15310 Attiki, Greece*

A. Blondel, G. Bonneaud, J.-C. Brient, A. Rougé, M. Rumpf, M. Swynghedauw, M. Verderi, H. Videau

*Laboratoire de Physique Nucléaire et des Hautes Energies, Ecole Polytechnique, IN$^2$P$^3$-CNRS, F-91128 Palaiseau Cedex, France*

E. Focardi, G. Parrini, K. Zachariadou

*Dipartimento di Fisica, Università di Firenze, INFN Sezione di Firenze, I-50125 Firenze, Italy*

R. Cavanaugh, M. Corden, C. Georgiopoulos

*Supercomputer Computations Research Institute, Florida State University, Tallahassee, FL 32306-4052, USA* [13,14]

A. Antonelli, G. Bencivenni, G. Bologna,[4] F. Bossi, P. Campana, G. Capon, V. Chiarella, P. Laurelli, G. Mannocchi,[1,5] F. Murtas, G.P. Murtas, L. Passalacqua, M. Pepe-Altarelli[1]

*Laboratori Nazionali dell'INFN (LNF-INFN), I-00044 Frascati, Italy*

L. Curtis, J.G. Lynch, P. Negus, V. O'Shea, C. Raine, P. Teixeira-Dias, A.S. Thompson

*Department of Physics and Astronomy, University of Glasgow, Glasgow G12 8QQ,United Kingdom*[10]

O. Buchmüller, S. Dhamotharan, C. Geweniger, P. Hanke, G. Hansper, V. Hepp, E.E. Kluge, A. Putzer,

J. Sommer, K. Tittel, S. Werner,[19] M. Wunsch

*Institut für Hochenergiephysik, Universität Heidelberg, D-69120 Heidelberg, Germany*[16]

R. Beuselinck, D.M. Binnie, W. Cameron, P.J. Dornan,[1] M. Girone, S. Goodsir, E.B. Martin, N. Marinelli, A. Sciabà, J.K. Sedgbeer, E. Thomson, M.D. Williams

*Department of Physics, Imperial College, London SW7 2BZ, United Kingdom*[10]

V.M. Ghete, P. Girtler, E. Kneringer, D. Kuhn, G. Rudolph

*Institut für Experimentalphysik, Universität Innsbruck, A-6020 Innsbruck, Austria*[18]

C.K. Bowdery, P.G. Buck, A.J. Finch, F. Foster, G. Hughes, R.W.L. Jones, N.A. Robertson, M.I. Williams

*Department of Physics, University of Lancaster, Lancaster LA1 4YB, United Kingdom*[10]

I. Giehl, K. Jakobs, K. Kleinknecht, G. Quast, B. Renk, E. Rohne, H.-G. Sander, H. Wachsmuth, C. Zeitnitz

*Institut für Physik, Universität Mainz, D-55099 Mainz, Germany*[16]

J.J. Aubert, C. Benchouk, A. Bonissent, J. Carr,[1] P. Coyle, F. Etienne, F. Motsch, P. Payre, M. Talby, M. Thulasidas

*Centre de Physique des Particules, Faculté des Sciences de Luminy, IN$^2$P$^3$-CNRS, F-13288 Marseille, France*

M. Aleppo, M. Antonelli, F. Ragusa

*Dipartimento di Fisica, Università di Milano e INFN Sezione di Milano, I-20133 Milano, Italy*

V. Büscher, H. Dietl, G. Ganis, K. Hüttmann, G. Lütjens, C. Mannert, W. Männer, H.-G. Moser, S. Schael, R. Settles, H. Seywerd, H. Stenzel, W. Wiedenmann, G. Wolf

*Max-Planck-Institut für Physik, Werner-Heisenberg-Institut, D-80805 München, Germany*[16]

P. Azzurri, J. Boucrot, O. Callot, S. Chen, A. Cordier, M. Davier, L. Duflot, J.-F. Grivaz, Ph. Heusse, A. Jacholkowska,[1] F. Le Diberder, J. Lefrançois, A.-M. Lutz, M.-H. Schune, J.-J. Veillet, I. Videau,[1] D. Zerwas

*Laboratoire de l'Accélérateur Linéaire, Université de Paris-Sud, IN$^2$P$^3$-CNRS, F-91898 Orsay Cedex, France*

G. Bagliesi, S. Bettarini, T. Boccali, C. Bozzi,[12] G. Calderini, R. Dell'Orso, I. Ferrante, L. Foà, A. Giassi, A. Gregorio, F. Ligabue, A. Lusiani, P.S. Marrocchesi, A. Messineo, F. Palla, G. Rizzo, G. Sanguinetti, G. Sguazzoni, R. Tenchini, C. Vannini, A. Venturi, P.G. Verdini

*Dipartimento di Fisica dell'Università, INFN Sezione di Pisa, e Scuola Normale Superiore, I-56010 Pisa, Italy*

G.A. Blair, G. Cowan, M.G. Green, T. Medcalf, J.A. Strong, J.H. von Wimmersperg-Toeller

*Department of Physics, Royal Holloway & Bedford New College, University of London, Surrey TW20 OEX, United Kingdom*[10]

D.R. Botterill, R.W. Clifft, T.R. Edgecock, P.R. Norton, J.C. Thompson

*Particle Physics Dept., Rutherford Appleton Laboratory, Chilton, Didcot, Oxon OX11 OQX, United Kingdom*[10]

B. Bloch-Devaux, P. Colas, S. Emery, W. Kozanecki, E. Lançon, M.-C. Lemaire, E. Locci, P. Perez, J. Rander, J.-F. Renardy, A. Roussarie, J.-P. Schuller, J. Schwindling, A. Trabelsi,[21] B. Vallage

*CEA, DAPNIA/Service de Physique des Particules, CE-Saclay, F-91191 Gif-sur-Yvette Cedex, France*[17]

S.N. Black, J.H. Dann, R.P. Johnson, H.Y. Kim, N. Konstantinidis, A.M. Litke, M.A. McNeil, G. Taylor

*Institute for Particle Physics, University of California at Santa Cruz, Santa Cruz, CA 95064, USA*[22]

C.N. Booth, S. Cartwright, F. Combley, M.S. Kelly, M. Lehto, L.F. Thompson

*Department of Physics, University of Sheffield, Sheffield S3 7RH, United Kingdom*[10]

K. Affholderbach, A. Böhrer, S. Brandt, C. Grupen, G. Prange

*Fachbereich Physik, Universität Siegen, D-57068 Siegen, Germany*[16]

G. Giannini, B. Gobbo

*Dipartimento di Fisica, Università di Trieste e INFN Sezione di Trieste, I-34127 Trieste, Italy*

J. Rothberg, S. Wasserbaech

*Experimental Elementary Particle Physics, University of Washington, WA 98195 Seattle, U.S.A.*

S.R. Armstrong, E. Charles, P. Elmer, D.P.S. Ferguson, Y. Gao, S. González, T.C. Greening, O.J. Hayes, H. Hu, S. Jin, P.A. McNamara III, J.M. Nachtman,[2] J. Nielsen, W. Orejudos, Y.B. Pan, Y. Saadi, I.J. Scott, J. Walsh, Sau Lan Wu, X. Wu, G. Zobernig

*Department of Physics, University of Wisconsin, Madison, WI 53706, USA*[11]

[1]Also at CERN, 1211 Geneva 23, Switzerland.

[2]Now at University of California at Los Angeles (UCLA), Los Angeles, CA 90024, U.S.A.

[3]Also at Centro Siciliano di Fisica Nucleare e Struttura della Materia, INFN, Sezione di Catania, 95129 Catania, Italy.

[4]Also Istituto di Fisica Generale, Università di Torino, 10125 Torino, Italy.

[5]Also Istituto di Cosmo-Geofisica del C.N.R., Torino, Italy.

[6]Supported by the Commission of the European Communities, contract ERBFMBICT982894.

[7]Supported by CICYT, Spain.

[8]Supported by the National Science Foundation of China.

[9]Supported by the Danish Natural Science Research Council.

[10]Supported by the UK Particle Physics and Astronomy Research Council.

[11]Supported by the US Department of Energy, grant DE-FG0295-ER40896.

[12]Now at INFN Sezione de Ferrara, 44100 Ferrara, Italy.

[13]Supported by the US Department of Energy, contract DE-FG05-92ER40742.

[14]Supported by the US Department of Energy, contract DE-FC05-85ER250000.

[15]Permanent address: Universitat de Barcelona, 08208 Barcelona, Spain.

[16]Supported by the Bundesministerium für Bildung, Wissenschaft, Forschung und Technologie, Germany.

[17]Supported by the Direction des Sciences de la Matière, C.E.A.

[18]Supported by Fonds zur Förderung der wissenschaftlichen Forschung, Austria.

[19]Now at SAP AG, 69185 Walldorf, Germany.

[20]Now at Harvard University, Cambridge, MA 02138, U.S.A.

[21]Now at Département de Physique, Faculté des Sciences de Tunis, 1060 Le Belvédère, Tunisia.

[22]Supported by the US Department of Energy, grant DE-FG03-92ER40689.

[23]Now at Université de Lausanne, 1015 Lausanne, Switzerland.

# 1 Introduction

In this paper measurements are presented of the hadronic structure function $F_2^\gamma$ of a quasi-real photon in deep inelastic electron-photon scattering. The function $F_2^\gamma$ describes much of our knowledge of the hadronic nature of the photon and as such is an important measurement, not only for its own sake, but also because it is used in analytical and Monte Carlo calculations of many processes both in two-photon physics and photoproduction.

In general, $F_2^\gamma$ is a function of the Bjorken variable $x$, the fractional momentum of the struck parton in the target photon, as well as $Q^2$ and $P^2$ which are the squared four-momenta transfered from the scattered leptons to the interacting virtual photons. In the experimental conditions considered here where only one of the scattered leptons is detected or "tagged" then one of the four-momentum transfers, taken to be $P$, is very close to zero and its influence need not be considered any further.

The cross section for the production of hadrons in deep inelastic electron-photon scattering depends on two hadronic structure functions $F_2^\gamma$ and $F_L^\gamma$. The differential cross section is [1]

$$\frac{\mathrm{d}^3\sigma}{\mathrm{d}y\,\mathrm{d}x\,\mathrm{d}Q^2} = \frac{4\pi\alpha^2}{Q^4 x}\left(1-y+\frac{y^2}{2}\right)\left[F_2^\gamma(x,Q^2) - \frac{y^2}{2(1-y+\frac{y^2}{2})}F_L^\gamma(x,Q^2)\right]\Phi(x,y). \quad (1)$$

where

$$Q^2 = 2EE'(1-\cos\theta), \quad (2)$$

$E$ is the energy of the incident beam, and $E'$ and $\theta$ are the energy and scattering angle of the scattered electron, respectively. The Bjorken variable $x$ is

$$x = \frac{Q^2}{2p\cdot q} = \frac{Q^2}{(Q^2+W^2+P^2)}, \quad (3)$$

where $p$ and $q$ are the four-momenta of the two virtual photons, $W$ is the total mass of the $\gamma^*\gamma$ system. The Bjorken variable $y$ is given by

$$y = \frac{qp}{k\cdot p} = 1 - \frac{E'}{2E}(1+\cos\theta), \quad (4)$$

where $k$ is the four-momentum of the incident electron or positron which scatters with high $Q^2$. The function $\Phi(x,y)$ is the flux of the target virtual photons radiated from the other incident electron or positron and is approximately given by [1]

$$\Phi \simeq \frac{\alpha}{y\pi}\left[\left(1-\frac{Q^2}{\mathcal{X}}+\frac{Q^4}{2\mathcal{X}^2}\right) ln\frac{P^2_{\max}}{P^2_{\min}} - \frac{m_e^2 Q^4}{\mathcal{X}^2}\left(\frac{1}{P^2_{\min}}-\frac{1}{P^2_{\max}}\right)\right] f(P^2), \quad (5)$$

where

$$\mathcal{X} = 4E^2xy, \quad (6)$$

and $P^2_{\min}$, and $P^2_{\max}$ are the minimum and maximum allowed values of $P^2$ and $m_e$ is the mass of the electron. The final factor $f(P^2)$ in this expression is the photon form factor.

In the Vector Dominance Model, the function $f(P^2)$ is expected to be close to unity for the values of $P^2$ encountered in the data considered here.

At experimentally accessible values of $y$, Eqn. 1 is insensitive to $F_L^\gamma(x,Q^2)$, so measurements of the cross-section for tagged two-photon physics provide a means to measure $F_2^\gamma$ . As originally described by Witten [2], the QCD expression for $F_2^\gamma$ divides into two parts. The first part is exactly calculable in perturbative QCD and is referred to as the "point-like" part. It becomes increasingly dominant at high $Q^2$ compared with the second contribution which is not calculable in perturbation theory and is known as the "hadronic" part. By analogy with nucleon structure functions, $F_2^\gamma$ can be expressed as the sum of momentum weighted densities of quarks "inside" the photon:

$$F_2^\gamma(x,Q^2) = \sum_{i=1}^{2f} x e_i^2 q_i^\gamma(x,Q^2) \tag{7}$$

where $f$ is the number of active flavours, $e$ is the charge of the quark and $q_i^\gamma(x,Q^2)$ is the photon parton density function 'PDF'. Several authors [3–12] have calculated $F_2^\gamma$ . Their predictions show the largest disagreements at low $x$, where the poorly known gluonic part of $F_2^\gamma$ is significant and can lead to a rapid rise in $F_2^\gamma$ . These calculations generally involve a degree of fitting to the measurements of the photon structure function existing at the time of the calculation. This means the more recent calculations are more tightly constrained than the earlier ones. For example the predictions of [11] and [12] had access to early LEP 1 data, whereas the others used only PETRA, PEP and KEK data, apart from the prediction of [4] which uses just one measurement from PLUTO [13]. A review of the current theoretical and experimental status of $F_2^\gamma$ is given in Ref. [14].

In this paper, $F_2^\gamma$ is extracted from the measured rates of hadron production in $\gamma^*\gamma$ interactions where the scattered electron tag is detected in the electromagnetic calorimeters.

# 2 Detector and Trigger

The ALEPH detector has been described in detail elsewhere [15, 16]. The key components for observing the final state products are the time projection chamber (TPC), the electromagnetic calorimeter (ECAL), and the hadron calorimeter (HCAL). The two luminosity calorimeters LCAL and SiCAL were used to measure the hadronic energy at small angles. The inner tracking chamber (ITC) while primarily designed to supply fast track triggers, provides additional information on charged tracks. The muon chambers, the outermost part of the detector, were used for muon identification. At scattering angles above 17.25 degrees, the combination of $\mathrm{d}E/\mathrm{d}x$ information from the TPC and the distribution of energy deposition in the calorimeters allows identification of high energy electrons [16]. At smaller angles no tracking information is available, but the backgrounds due to Z decays are relatively smaller and so large energy electromagnetic showers can be reliably assumed to be due to scattered electrons from two photon scattering processes. Reconstruction of the final state of the event uses the energy flow objects [17] which consist of charged tracks, identified photons, and neutral hadrons.

The details of the trigger are given in Ref. [16]. In the 9% of events tagged in the ECAL, both the tag itself and the hadronic final state are capable of triggering the event, which ensures 100% trigger efficiency for these events. For the remaining events where the tag is observed in the LCAL the event must be triggered by the hadronic final state since the whole detector is not routinely read out for events triggered in LCAL. In 92% of these events the trigger requires a single low energy track defined by a coincidence between a track as defined by the ITC and an energy deposit of more than 200 MeV in the ECAL. Other triggers which are fired in a significant number of events require either two approximately back to back tracks in the ITC or an energy deposit in the ECAL with a higher energy threshold.

For events with many high momentum tracks the single track trigger is essentially 100% efficient. However for events with only a few low momentum tracks such as in this analysis, this may no longer be the case. The other triggers involve at least one component in common with the main single track trigger, and so the normal method of measuring trigger efficiency by comparing two independent triggers is not available. In view of this, an alternative method was adopted to measure the efficiency of the single track trigger. For this purpose a special selection was made on the data which required the presence of just a single track. These events set either the single track trigger or another independent trigger such as those using LCAL or SiCAL information, or both. By comparing the rates for each trigger it was possible to derive the efficiency for the single track trigger as a function of the transverse momentum of a track with respect to the beam direction. This function was then used on an event-by-event basis to calculate the trigger efficiency of a given event. It resulted in an efficiency of 98% for low $x_{\rm vis}$, falling to 94% for high $x_{\rm vis}$, in LCAL tagged events, where $x_{\rm vis}$ is the measured value of $x$, calculated from the observed final state particles. In the remainder of this analysis all events have been weighted using this efficiency.

The triggers which are important for this analysis are also those most susceptible to triggering on unwanted background from the LEP beam, and detector noise so they were were downscaled by varying amounts during the LEP 1 data taking period. All events have been weighted as appropriate to correct for the trigger efficiencies and downscaling, resulting in a mean weight for the LCAL tagged events of 1.09.

# 3 Data Selection

This analysis uses the ALEPH data taken between 1991–1995. The LEP beam energy in this period was between 44 and 47 GeV, with a mean of 45.6 GeV. A total integrated luminosity of 162 (155) pb$^{-1}$ was used for the ECAL (LCAL) tagged events. The number of $\gamma^*\gamma$ collisions expected in this sample is a few thousand, compared with the 4.9 million Z decays detected in the same period. The purpose of the data selection procedure is to extract a clean sample of hadronic $\gamma^*\gamma$ scattering events, free from background due to Z decays and leptonic $\gamma\gamma$ processes.

Events were selected in which the scattered electron was detected in either the ECAL or LCAL calorimeters. In the case of the ECAL, a tag was defined to be an identified electron

with energy greater than 12 GeV, with a scattering angle whose cosine was less than 0.95 and greater than $-0.6$. For the LCAL tagged events, a cluster of energy greater than 30 GeV, with a scattering angle between 65 and 150 mrad was taken to be an electron. A cone was constructed around the electron defined by a half angle of $\cos^{-1} = 0.995$ and identified photons within this cone were added to the electron four-momentum to form the final tag. To ensure that events used in this analysis were genuinely single-tagged, an event was required to contain just one tag where the definition of a tag was broadened for this purpose to include clusters in the SiCAL and LCAL with energy greater than 20 GeV.

The following cuts were then applied to eliminate background events (mainly from Z decays). To eliminate the majority of $\mathrm{Z} \to f\bar{f}$ events the following requirements were applied:

- The number of energy flow objects of all types must be less than 26.
- $W_{\mathrm{vis}}$ must be less than 40 GeV/$c^2$. $W_{\mathrm{vis}}$ is defined as the value of $W$ reconstructed from the observed hadronic final state particles.
- The normalised longitudinal momentum balance (NLMB) [18] must be greater than 0.2 (in ECAL tagged events), or 0.3 (in LCAL tagged events), where

$$\mathrm{NLMB} = \frac{\cos\theta\,\Sigma p_z}{|\cos\theta|\,\Sigma E}$$

  and $\theta$ is the angle of the tagged electron with respect to the beam direction. $\Sigma E$ and $\Sigma p_z$ are respectively the sums of the energies and $z$ components of momentum of all energy flow objects in the event, including the tag. The $z$ direction corresponds to the beam direction.
- There must be no energy flow object closer than 11.5 degrees from the tag.
- The total energy in a cone opposite in direction to the tag, with an opening angle of 18.2 degrees, must be less than 20 GeV.

Specific cuts against $\mathrm{Z} \to \mu^+\mu^-, e^+e^-$ were then imposed:

- The total electromagnetic energy in identified photons and electrons (excluding the tag) must be less than 20 GeV.
- Apart from the tagged electron, there must be no identified electron or muon of momentum greater than 2 GeV/$c$.

The remaining $\mathrm{Z} \to \tau^+\tau^-$ and $\gamma^*\gamma \to l^+l^-$ events were removed by the following condition:

- The number of charged tracks must be greater than 2.
- $W_{\mathrm{vis}}$ must be greater than 2 GeV/$c^2$.
- Events with fewer than six charged tracks must have a thrust value less than 0.985.

Table 1: Background fraction for significant physics processes in each $Q^2$ bin calculated by Monte Carlo simulation.

| | Background fraction (%) | | |
|---|---|---|---|
| Background process | $\langle Q^2 \rangle$ (GeV$^2$) 9.9 | 20.7 | 284.0 |
| $\gamma^*\gamma \to \tau^+\tau^-$ | 4.6 | 6.5 | 7.8 |
| $Z \to q\bar{q}$ | 2.1 | 3.5 | 4.3 |
| $Z \to \tau\bar{\tau}$ | 0.0 | 0.0 | 1.9 |

To eliminate beam gas events, the interaction point must be reconstructed within 6 cm in the $z$ direction and 1 cm in the radial direction from the nominal interaction point.

The total number of surviving ECAL tagged events in the data was 163. The data cover the range $35 < Q^2 < 3000$ GeV$^2$ with a mean value of $Q^2$ of $284 \pm 49$ GeV$^2$. The LCAL data were split into two samples. One sample consists of 1543 events in the range $6 < Q^2 < 13$, and a mean $Q^2$ of $9.93 \pm 0.04$ GeV$^2$. The other sample contains 1647 events in the $Q^2$ range $13 < Q^2 < 44\,\mathrm{GeV}^2$ with a mean of $20.67 \pm 0.16$ GeV$^2$.

The size of the background contribution from all known sources has been determined for each sample using Monte Carlo simulations. Table 1 shows the expected fraction of events for the only significant sources of background. All other background processes are found to be at a level of less than 1% and are neglected. For the ECAL tagged events the detection efficiencies are similar for high energy electrons and muons in the regions covered by this analysis [16]. This allowed a direct measurement of the background in the data due to Z decay by repeating the data selection with the tag electron replaced by an identified muon. This resulted in a sample of 11 events (6.7%) which is in good agreement with that determined from the simulations of Z decays (6.2%) (Table 1). The background to the ECAL tagged sample was calculated by taking the average of the muon tagged and Monte Carlo simulated events. The background (Table 1) from the process $\gamma^*\gamma \to \tau^+\tau^-$ was subtracted using simulated events.

# 4 Comparison with Models

The invariant mass $W$ in $\gamma^*\gamma$ events is in general poorly measured by current detectors due to the significant proportion of the energy of the event which goes in the forward region where there is little or no tracking information. Therefore extraction of a measurement of the photon structure function from the data depends on the use of a model of the production of hadronic final states from $\gamma^*\gamma$ collisions. There is at present no complete theoretical description of this process, so a number of phenomenological models are used.

The conventional approach to modelling the production of hadrons in $\gamma^*\gamma$ interactions is to combine models based on the Quark Parton Model (QPM) and the Vector Meson Dominance Model, (VDM) [19]. Recently it has also become possible to use standard

generators such as HERWIG [20].

For the VDM component of the conventional QPM+VDM approach the simulation of VDM described in Ref. [23] was used. The hadronic part of the photon, simulated by VDM, is assumed to have a cross section for $\gamma^*\gamma$ scattering of the form

$$\frac{\mathrm{d}\sigma_{\gamma^*\gamma}}{\mathrm{d}Q^2\,\mathrm{d}P^2\,\mathrm{d}W^2} = \left(A + \frac{B}{W}\right) f(Q^2) f(P^2), \tag{8}$$

where $A$ and $B$ are determined from the data as described below. The form of $f(P^2)$ is chosen to be the Generalised Vector Dominance Model (GVDM) form [21], which generally provides a better description of photon processes than the simpler $\rho$ pole formulation [22]. The Generalised VDM form factor $f(Q^2)$ is given by

$$f(Q^2) = \Sigma R_i \frac{1 + Q^2/4M_i^2}{(1 + Q^2/M_i^2)^2} + \frac{0.22}{1 + Q^2/1.96}, \tag{9}$$

where the summation is taken over three vector mesons of masses $M_i$ equal to those of the $\rho$, $\omega$ and $\phi$ and the constants $R_i$ are 0.65, 0.08 and 0.05. The QPM generator used for this analysis is the program of Berends, Darveveldt and Kleiss (BDK) [24], which includes processes in which additional photons are radiated from the incoming and outgoing electrons. It was used to produce events containing quarks with transverse momentum greater than 2 GeV/$c$ with respect to the $\gamma^*\gamma$ direction.

The hadronisation process was handled in both QPM and VDM by the JETSET program [25]. The quarks were first allowed to radiate gluons via the Lund parton shower scheme. In the QPM case, $Q_{\max}$, the maximum scale for the shower, was set to $W$, the invariant mass of the final state. This was found to slightly improve the description of the charged multiplicity in the ECAL tagged events compared to a model where no gluon radiation was allowed. In the VDM model $Q_{\max}$ was set to the $p_t$ of the quarks with respect to the $\gamma^*\gamma$ direction. In practice this suppresses any gluon radiation. The resulting partons were then passed to the string fragmentation program for production of the final state hadrons.

The QPM sample was combined with the VDM sample to form a single set, weighting each sample so as to give the best overall value of $\chi^2$ between the distributions predicted by the combined simulation and the data. The distributions used in this procedure were the number of energy flow objects, the transverse momentum of all energy flow objects with respect to the beam direction, and the thrust of the event.

An alternative simulation was produced, using the HERWIG program with the GRV LO photon parton density function [8]. All parameters of the program were set at their defaults for version 5.9, apart from the intrinsic transverse momentum $k_t$ of the partons in the target photon. This was modified according to the scheme described in Ref. [26] where the $k_t$ distribution is made broader than the default using a power-like distribution originally proposed by the ZEUS [27] collaboration to describe their photoproduction data.

Comparisons between the data and the two sets of simulated events are presented in Figs. 1 and 2. The HERWIG sample is normalised to the number of events in the data. This is equivalent to a cross section 20% larger than that predicted by the program. In general both models give an acceptable description of the data.

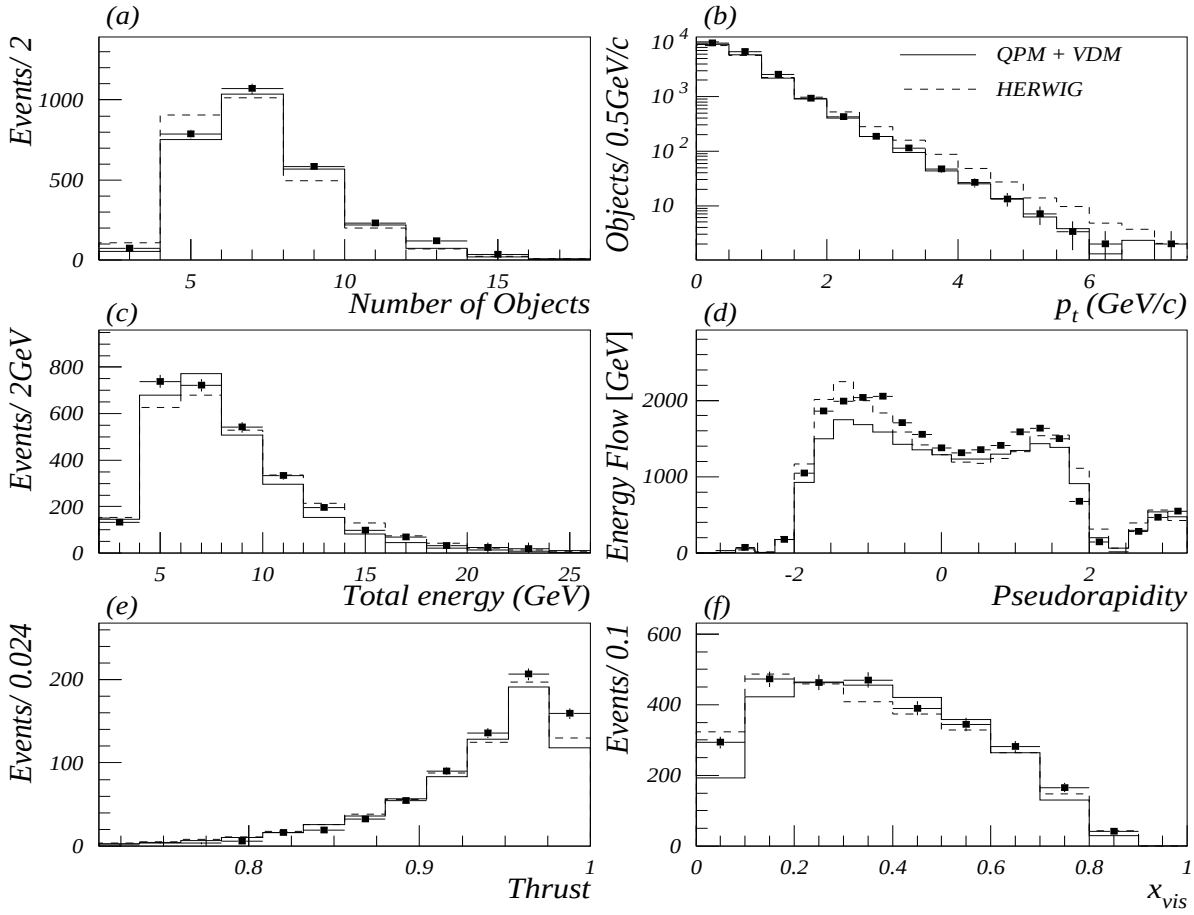


Figure 1: Comparison of data and simulations for LCAL tagged data. The points with error bars are the data, the solid histogram is the QPM+VDM model and the dashed histogram is the HERWIG model. The plots are (a) number, (b) $p_t$ with respect to beam direction, and (c) total energy of the final state energy flow objects. Plot (d) is the energy weighted pseudorapidity distribution. The pseudorapidity $\eta$ is defined as $\eta = -\ln(\tan(\theta'/2))$ where $\theta'$ is the angle of an energy flow object with respect to the beam which radiates the target photon. With this definition the tag lies in the negative $\eta$ direction but is not included. Plot (e) is the thrust calculated from the final state energy flow objects and (f) is the $x_{\rm vis}$ distribution used to extract the measurement of $F_2^\gamma$.

# 5 Extraction of the Structure Function $F_2^\gamma(x)$

Integrating Eqn. 1 over $y$ and $Q^2$ gives an expression for $\mathrm{d}\sigma/\mathrm{d}x$ in terms of the structure functions $F_2^\gamma(x)$ and $F_L^\gamma(x)$. As shown in Fig. 3, the measured value $x_{\rm vis}$ is smeared asymmetrically from the true value so that an unfolding procedure is first necessary to extract the true $x$ distributions from the data. The unfolding was performed using the procedure proposed by Blobel [28]. This procedure fits a sum of spline curves to the data after passing them through the $x_{\rm vis}$ versus $x_{\rm true}$ matrix obtained from the simulated events. A regularisation procedure is used to suppress oscillations in the result which have higher frequency than are justified by the resolution of the input measurements. It is important later in this analysis to ensure a reliable measurement at low $x$, where the

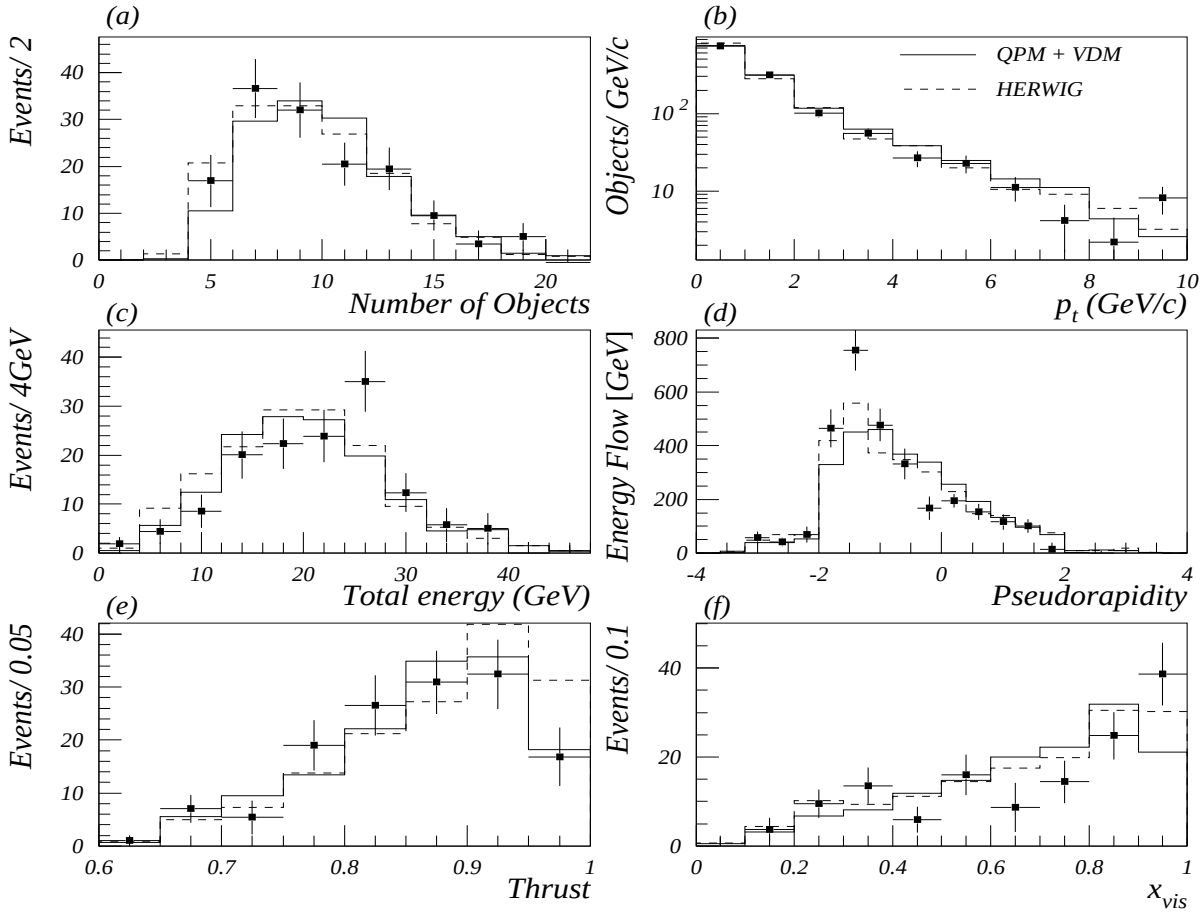


Figure 2: The same as Fig. 1 but for ECAL tagged data.

greatest discrepancy is seen between different theoretical predictions of $F_2^\gamma(x)$ . For this reason the low edge in $x$ is defined as the point where the efficiency reaches 1/3 of its maximum value. At high $x$ the efficiency falls off slowly. The maximum $x$ is chosen to be the point at which the efficency has fallen to zero. Within these limits the number of bins and their ranges are those recommended by the unfolding procedure so as to minimise the bin to bin correlation of the results. The unfolding was performed twice, once for each of the two models (HERWIG and QPM+VDM). There were in all cases at least five times as many simulated events as real ones. The final results presented below are the means of the results obtained in each case. For each bin the mean value of $x$ in the bin was calculated using the functional form of $\mathrm{d}\sigma/\mathrm{d}x$ returned by the unfolding procedure.

The measured values of $\mathrm{d}\sigma/\mathrm{d}x$ are presented in Table 2. A measurement of $F_2^\gamma$ can be obtained from the measured values of $\mathrm{d}\sigma/\mathrm{d}x$ by dividing the measurement in a given bin by the integral of Eqn. 1 having first set $F_L^\gamma(x,Q^2)$ to its theoretical value. Currently the only available prediction for $F_L(x,Q^2)$ [14] is that given by the QPM. In practice, in the data analysed here, the value of $y$ is sufficiently small that the coefficient that multiplies $F_L^\gamma(x,Q^2)$ in Eqn. 1 much reduces its contribution to $\mathrm{d}\sigma/\mathrm{d}x$. The GALUGA program [29]

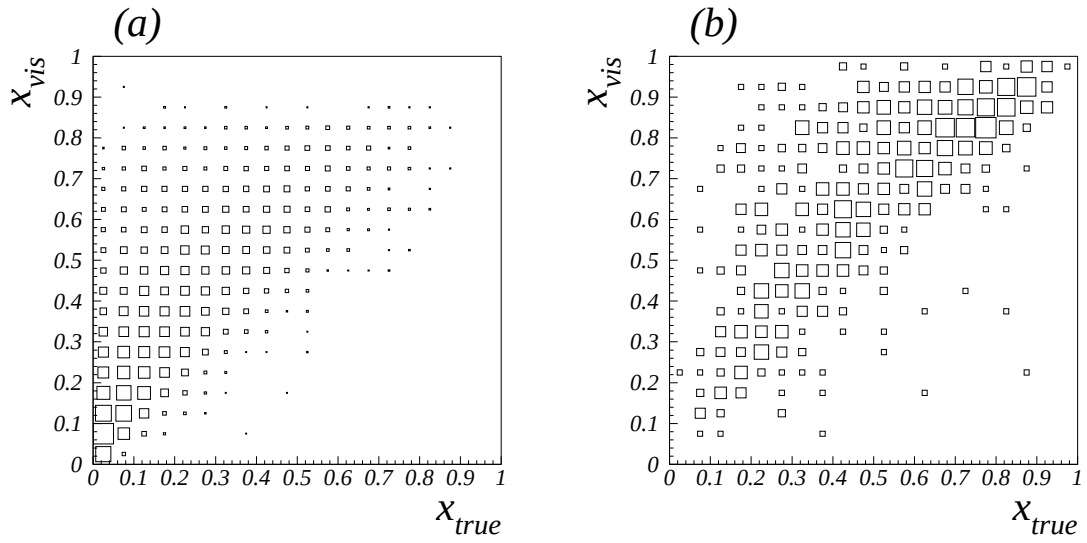


Figure 3: $x_{\rm vis}$ versus $x_{\rm true}$ for (a) LCAL tagged and (b) ECAL tagged events simulated by the HERWIG program.

can be used to calculate Eqn. 1 exactly, so it was used to calculate the theoretical value for $\mathrm{d}\sigma/\mathrm{d}x$ in the $x$ and $Q^2$ bins used in this analysis. The resulting measurements of $F_2^\gamma(x)$ are listed in Table 3. Table 4 shows the bin to bin correlations of the results.

To study the dependence of $F_2^\gamma$ with $Q^2$ it is convenient to analyse the data in a fixed $x$ bin. The region $0.1 < x < 0.6$ is chosen, so as to remove the regions at low and high $x$ where the greatest theoretical uncertainty arises, but at the same time to ensure as precise a measurement as possible in all the $Q^2$ bins used. The results obtained in this way are most suitable for testing the $\log(Q^2)$ dependence predicted by QCD. Table 5 shows the value of $F_2^\gamma$ in this range.

# 6 Systematic errors

The contributions to the systematic errors are listed in Table 2. Differences between the results obtained with the two models could derive either from a dependence of the result on the structure function used in the Monte Carlo or from differences in the hadronisation schemes.

The LAC 1 [5] structure function shows the most rapid rise at low $x$ of any available set. The standard HERWIG sample used GRV LO which has a much less rapid increase at small $x$. To measure the effect on the unfolding of varying the input PDF, the standard HERWIG sample was reweighted by the ratio of the structure function calculated using the LAC 1 PDF and the GRV LO PDF. Comparing the result of unfolding using this sample to that obtained using the unweighted HERWIG sample measures the effect of varying the input PDF. So as to measure the dependence of the result on the hadronisation process, the unfolding was performed using the QPM+VDM sample reweighted to have the same

Table 2: The measured values of $\mathrm{d}\sigma/\mathrm{d}x$ in three $Q^2$ bins.

| $\langle Q^2 \rangle = 284$ GeV$^2$ | | | |
|---|---|---|---|
| $x$ range | $0.03 - 0.35$ | $0.35 - 0.65$ | $0.65 - 0.97$ |
| $\langle x \rangle$ | 0.171 | 0.50 | 0.80 |
| $\mathrm{d}\sigma/\mathrm{d}x$ (pb) | 4.1 | 2.4 | 3.1 |
| Statistical error | 0.7 | 0.6 | 0.6 |
| Hadronisation uncertainty | 0.5 | 0.6 | 0.6 |
| Detector Simulation uncertainty | 0.2 | 0.2 | 0.2 |
| Theoretical error | 0.2 | 0.1 | 0.1 |
| Total error | 0.9 | 0.8 | 0.9 |

| $\langle Q^2 \rangle = 20.7$ GeV$^2$ | | | | |
|---|---|---|---|---|
| $x$ range | $0.009 - 0.12$ | $0.12 - 0.27$ | $0.27 - 0.50$ | $0.50 - 0.89$ |
| $\langle x \rangle$ | 0.055 | 0.19 | 0.38 | 0.63 |
| $\mathrm{d}\sigma/\mathrm{d}x$ (pb) | 79.1 | 41.5 | 45.8 | 22.2 |
| Statistical error | 5.4 | 4.1 | 4.2 | 5.2 |
| Hadronisation uncertainty | 10.3 | 13.3 | 8.2 | 0.2 |
| Detector Simulation uncertainty | 1.4 | 2.0 | 0.7 | 1.0 |
| Trigger uncertainty | 1.0 | 0.5 | 0.5 | 2.0 |
| Theoretical error | 0.8 | 0.4 | 0.5 | 0.2 |
| Total error | 11.8 | 14.0 | 9.3 | 5.7 |
| $\langle Q^2 \rangle = 9.9$ GeV$^2$ | | | | |
| $x$ range | $0.005 - 0.08$ | $0.08 - 0.20$ | $0.20 - 0.40$ | $0.40 - 0.80$ |
| $\langle x \rangle$ | 0.039 | 0.14 | 0.28 | 0.54 |
| $\mathrm{d}\sigma/\mathrm{d}x$ (pb) | 170.0 | 102.7 | 66.7 | 22.4 |
| Statistical error | 9.5 | 7.3 | 7.8 | 10.4 |
| Hadronisation uncertainty | 11.9 | 16.4 | 11.3 | 1.8 |
| Detector Simulation uncertainty | 6.1 | 3.9 | 8.6 | 6.4 |
| Trigger uncertainty | 1.7 | 1.0 | 4.0 | 3.6 |
| Theoretical error | 1.7 | 1.0 | 0.7 | 0.2 |
| Total error | 16.6 | 18.5 | 16.7 | 12.9 |

$x_{\mathrm{true}}$ distribution as the HERWIG sample and compared to that sample. A smooth $x_{\mathrm{vis}}$ distribution that matched the data was used in the estimate of this systematic error to avoid any influence from statistical fluctuations in the data. The dominant effect comes from the hadronisation process in all but the lowest $x$ bin of the lowest $Q^2$ set, where the influence of the input structure function is more significant. The quadratic sum of these two errors is referred to as the hadronisation uncertainty in Table 2.

The systematic error due to the simulation of the detector was checked by increasing

Table 3: The structure function $F_2^\gamma(x)/\alpha$ in three $Q^2$ bins.

| $\langle Q^2 \rangle = 284$ GeV$^2$ | | | |
|---|---|---|---|
| $x$ range | $0.03 - 0.35$ | $0.35 - 0.65$ | $0.65 - 0.97$ |
| $\langle x \rangle$ | 0.171 | 0.50 | 0.80 |
| $F_2^\gamma/\alpha$ | 0.65 | 0.70 | 1.28 |
| Statistical error | 0.10 | 0.16 | 0.26 |
| Systematic error | 0.09 | 0.19 | 0.26 |
| Total error | 0.14 | 0.25 | 0.37 |

| $\langle Q^2 \rangle = 20.7$ GeV$^2$ | | | | |
|---|---|---|---|---|
| $x$ range | $0.009 - 0.12$ | $0.12 - 0.27$ | $0.27 - 0.50$ | $0.50 - 0.89$ |
| $\langle x \rangle$ | 0.055 | 0.19 | 0.38 | 0.63 |
| $F_2^\gamma/\alpha$ | 0.36 | 0.34 | 0.56 | 0.45 |
| Statistical error | 0.02 | 0.03 | 0.05 | 0.11 |
| Systematic error | 0.05 | 0.11 | 0.10 | 0.05 |
| Total error | 0.05 | 0.12 | 0.11 | 0.12 |
| $\langle Q^2 \rangle = 9.9$ GeV$^2$ | | | | |
| $x$ range | $0.005 - 0.08$ | $0.08 - 0.20$ | $0.20 - 0.40$ | $0.40 - 0.80$ |
| $\langle x \rangle$ | 0.039 | 0.14 | 0.28 | 0.54 |
| $F_2^\gamma/\alpha$ | 0.30 | 0.40 | 0.41 | 0.27 |
| Statistical error | 0.02 | 0.03 | 0.05 | 0.13 |
| Systematic error | 0.02 | 0.07 | 0.09 | 0.09 |
| Total error | 0.03 | 0.07 | 0.10 | 0.16 |

Table 4: Bin to bin correlations in the $\langle Q^2 \rangle$= (a) 284, (b) 20.7, and (c) 9.9 GeV$^2$ results.

(a)

| Bin | 1 | 2 | 3 |
|---|---|---|---|
| 1 | 1.00 | −0.28 | −0.01 |
| 2 | | 1.00 | −0.33 |
| 3 | | | 1.00 |

(b)

| Bin | 1 | 2 | 3 | 4 |
|---|---|---|---|---|
| 1 | 1.00 | −0.33 | −0.06 | 0.04 |
| 2 | | 1.00 | −0.39 | 0.06 |
| 3 | | | 1.00 | −0.48 |
| 4 | | | | 1.00 |

(c)

| Bin | 1 | 2 | 3 | 4 |
|---|---|---|---|---|
| 1 | 1.00 | −0.21 | −0.09 | 0.07 |
| 2 | | 1.00 | −0.42 | 0.08 |
| 3 | | | 1.00 | −0.52 |
| 4 | | | | 1.00 |

Table 5: The mean value of $F_2^\gamma/\alpha$ in the range $0.1 < x < 0.6$.

| $Q^2$ (GeV$^2$) | 9.9 | 20.7 | 284 |
|---|---|---|---|
| $\langle F_2^\gamma/\alpha \rangle$ | 0.38 | 0.50 | 0.68 |
| Statistical error | 0.03 | 0.02 | 0.10 |
| Hadronisation uncertainty | 0.04 | 0.04 | 0.07 |
| Theory error | 0.00 | 0.00 | 0.03 |
| Total error | 0.05 | 0.05 | 0.12 |

the minimum energy of the energy flow objects included in the selection on both real and simulated events. The detector simulation error listed in Table 2 is either half the difference between the maximum and minimum values found as a result of these changes, or the statistical error due to the events that are lost by making the changes whichever is the larger. An additional systematic error is included which allows for the uncertainty in measuring the trigger efficiency. This was obtained by repeating the analysis but assuming 100% trigger efficiency. The uncertainty was then taken as the difference between this result and that obtained using the trigger efficiency calculated as described in section 2.

Two sources of theoretical error have been studied. The first of these was obtained by changing the form factor assumed for the target photon from the default GVDM form to a "rho pole" form factor. The second was the effect of the unknown contribution from $F_L^\gamma(x, Q^2)$. To test the dependence of the result on $F_L^\gamma(x, Q^2)$, its normalisation was varied in GALUGA between 0.5 and 2.0 times the QPM prediction. The theory error listed in Table 2 is the quadratic sum of these two contributions.

# 7 Comparison of $F_2^\gamma$ to Parametrisations

Figure 4 shows the values of $F_2^\gamma$ as a function of $x$. The inner error bars show the statistical errors and the outer error bars represent the total errors from adding the statistical and systematic errors in quadrature. The data are plotted at the mean $x$ position, and the horizontal bars show the bin width. Also shown are three representative parametrisations AFG HO [10],LAC 1, and GRV LO.

Table 6 shows the $\chi^2$ values obtained comparing this data to the more recent parametrisations of the parton density functions of the photon. The data are compatible with many of the parametrisations. Those that show significantly large values of $\chi^2$, such as LAC 1 and 2 and WHIT 4, 5, and 6, contain a large gluon content, resulting in a rapid rise in the structure function at low $x$.

To check whether the data would be sensitive to the presence of a rapid rise in $F_2^\gamma(x)$ at low $x$ the analysis was repeated, but with the data replaced by a sample of events simulated by HERWIG using the LAC 1 structure function. As expected, the lowest $x$ points in the LCAL tagged events were higher than those seen in the data, and repeating the $\chi^2$ test showed that such a measurement would find the LAC 1 and 2, and WHIT 4,

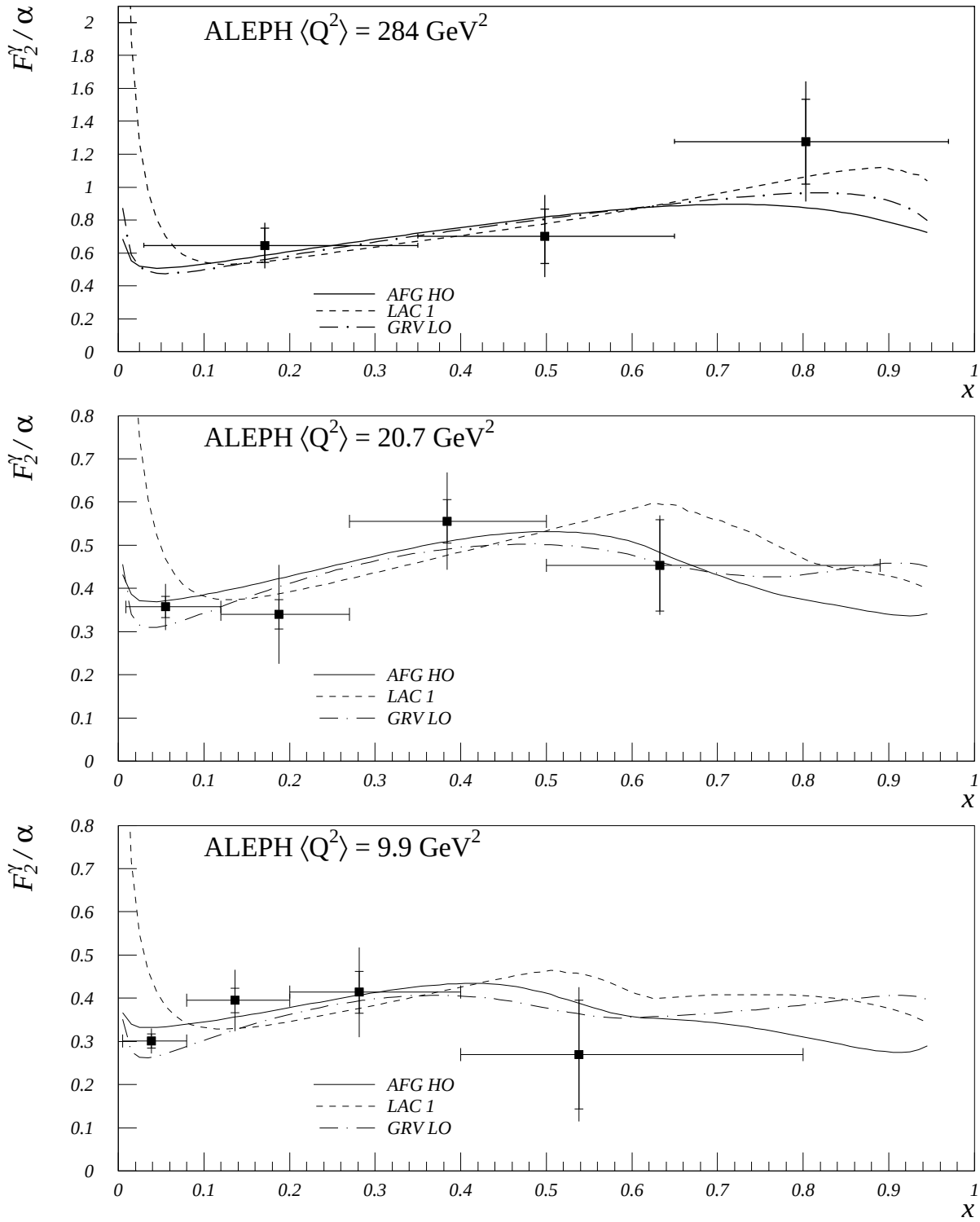


Figure 4: The values of $F_2^\gamma(x)/\alpha$ compared to three parametrisations.

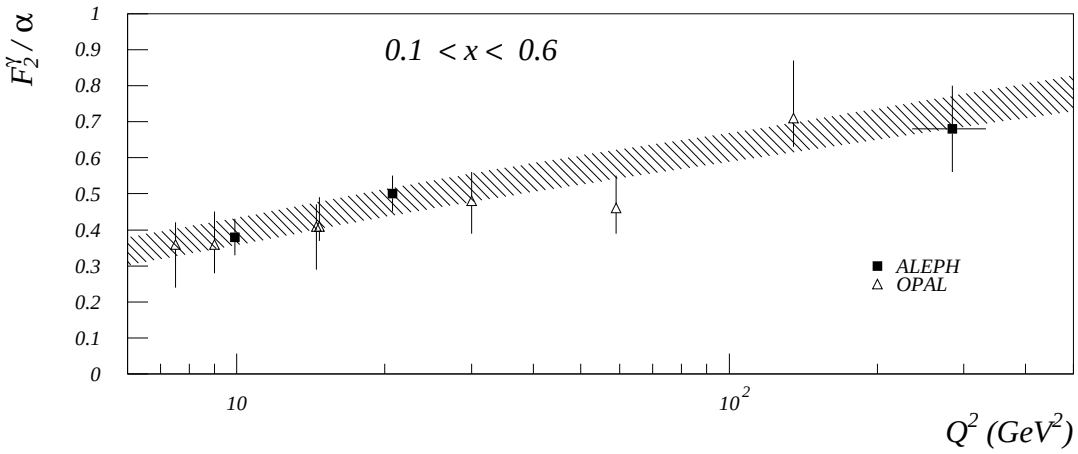


Figure 5: The values of $F_2^\gamma$ averaged over the region $0.1 < x < 0.6$. The band indicates the range of theoretical predictions obtained using the parametrisations listed in Table 6. Also shown are recent OPAL results [31] for the same $x$ range.

5 and 6 parametrisations to be highly favoured while rejecting all others.

The result for $F_2^\gamma$ in the range $0.1 < x < 0.6$ is compared to theoretical expectations and recent OPAL results [31] in Fig. 5. There is good agreement between the ALEPH and OPAL measurements, which are compatible with the theoretical predictions.

Table 6: The values of $\chi^2$ obtained comparing this data to the more recently calculated photon parton density functions (PDF). The leading order sets were obtained from the PDFLIB library [30]. The higher order sets were calculated with the assistance of the corresponding authors. The mnemonics for each PDF are taken from the PDFLIB manual.

| PDF | $\chi^2$ | PDF | $\chi^2$ |
|---|---|---|---|
| DG Set 1 [4] | 4.3 | DG Set 2 | 5.0 |
| LAC 1 [5] | 107.2 | LAC 2 | 75.9 |
| LAC 3 | 3.9 | GS-96 HO [7] | 7.6 |
| GS-96 LO | 8.9 | GRV HO [8] | 4.9 |
| GRV LO | 3.8 | AFG HO [10] | 4.6 |
| WHIT 1 [11] | 5.2 | WHIT 2 | 13.9 |
| WHIT 3 | 18.3 | WHIT 4 | 40.0 |
| WHIT 5 | 105.5 | WHIT 6 | 130.8 |
| SAS Set 1D [12] | 10.0 | SAS Set 1M | 4.3 |
| SAS Set 2D | 3.6 | SAS Set 2M | 3.7 |

# 8 Conclusions

Inclusive production of hadrons in $\gamma^*\gamma$ interactions has been studied using ALEPH data taken between 1991 and 1995. The results are presented in three bins of $Q^2$ which have a mean of 9.9, 20.7 and 284 GeV$^2$. The data have been used to measure the hadronic photon structure function $F_2^\gamma$ as a function of $x$. Comparisons to parametrised parton density functions show that those containing a large gluon content are inconsistent with the data. When the value of $F_2^\gamma$ in the range $0.1 < x < 0.6$ is plotted as function of $Q^2$ it is found to be compatible with the available parametrisations.

# Acknowledgements

We would like to thank A. Vogt, M. Fontannaz, and L. Gordon for help in calculating $F_2^\gamma$ for the GRV, AFG and GS parametrisations, respectively, and G. Schuler for useful discussions concerning the GALUGA program. We would like to thank our colleagues of the accelerator divisions at CERN for the outstanding performance of the LEP machine. Thanks are also due to the many engineers, and technical personnel at CERN and at the home institutes for their contribution to ALEPH's success. Those of us not from member states wish to thank CERN for its hospitality.

# References

[1] V.M. Budnev, I.F. Ginzburg, G.V. Meledin, and V.G. Serbo, *Phys. Rep.* **C15** (1975) 181.

[2] E.Witten *Nucl. Phys.* **B120** (1977) 189.

[3] D.W. Duke and J.F. Owens, *Phys. Rev.* **D26** (1982) 1600.

[4] M. Drees and K. Grassie, *Z. Phys.* **C28** (1985) 451.

[5] H. Abramowicz, K. Charchula and A. Levy, *Phys. Lett.* **B269** (1991) 458.

[6] L.E. Gordon and J.K. Storrow, *Z. Phys.* **C56** (1992) 307.

[7] L.E. Gordon and J.K. Storrow, *Nucl. Phys.* **B489** (1997) 405.

[8] M. Glück, E. Reya and A. Vogt, *Phys. Rev.* **D45** (1992) 3986; **D46** (1992) 1974.

[9] P. Aurenche et al., *Z. Phys.* **C56** (1992) 589.

[10] P. Aurenche, M. Fontannaz, J.Ph. Guillet, *Z. Phys.* **C64** (1994) 621.

[11] K. Hagiwara et al., *Phys. Rev.* **D51** (1995) 3197.

[12] G.A. Schuler and T. Sjöstrand, *Z. Phys.* **C68** (1995) 607.

[13] Ch. Berger et al., *Phys. Lett.* **B107** (1981) 168.

[14] M. Krawczyk, A. Zembrzuski, and M. Staszel, DESY 98-013, hep-ph/9806291.

[15] ALEPH Collaboration, *"ALEPH: a detector for electron-positron annihilation at LEP"*, *Nucl. Instr. Meth.* **A294** (1990) 121.

[16] ALEPH Collaboration, *"Performance of the ALEPH detector at LEP"*, *Nucl. Instr. Meth.* **A360** (1995) 481.

[17] ALEPH Collaboration, *"Searches for the standard Higgs boson"*, *Phys. Lett.* **B246** (1990) 306.

[18] JADE Collaboration, *"Experimental Study of the Photon Structure Function $F_2$ at $Q^2$ from 10 to 220* $\mathrm{GeV}^2$*"*, *Z. Phys.* **C24** (1984) 231.

[19] Ch. Berger and W. Wagner, *Phys. Rep.* **146** (1987) 1.

[20] G. Marchesini et al., *Computer Phys. Commun.* **67** (1992) 465.

[21] I.F. Ginzberg and V.G. Serbo, *Phys. Lett.* **B109** (1982) 231.

[22] PLUTO Collaboration, *"A measurement of the $Q^2$ and W Dependence of the $\gamma\gamma$ Total Cross Section for Hadron Production"*, *Z. Phys.* **C26** (1984) 353;
TPC/Two-Gamma Collaboration, *"Measurement of the total hadronic cross section in tagged $\gamma\gamma$ reactions"*, *Phys. Rev.* **D41** (1990) 2667;
CELLO Collaboration, *"Studies of multihadronic final states in photon-photon interactions"*, *Z. Phys.* , **C51** (1991) 365.

[23] ALEPH Collaboration, *"An experimental study of $\gamma\gamma \rightarrow$hadrons at LEP"*, *Phys. Lett.* **B313** (1993) 509.

[24] F.A. Berends, P.H. Daverveldt and R. Kleiss, *Computer Phys. Commun.* **40** (1986) 285.

[25] T. Sjöstrand, *Computer Phys. Commun.* **82** (1994) 74.

[26] The UK phenomenology workshop on LEP2 physics, S. Cartwright et al., *J. Phys. G* **24** (1998) 457.

[27] ZEUS Collaboration, *"Study of the photon remnant in resolved photoproduction at HERA"*, *Phys. Lett.* **B354** (1995) 163.

[28] V. Blobel, in Proceedings of the CERN School of Computing, Aiguablava, Spain (1984), CERN 85-09.

[29] G.A. Schuler, *Computer Phys. Commun.* **108** (1998) 279.

[30] H. Plothow-Besch, *Computer Phys. Commun.* **75** (1993) 396.

[31] OPAL Collaboration, *"Measurements of the $Q^2$ evolution of the photon structure function $F_2^\gamma$ "*, *Phys. Lett.* **B411** (1997) 387.